Jordan Journal of Physics

REVIEW ARTICLE

Computational Condensed Matter Physics: Progress and Prospects

Abdallah Qteish

Department of Physics, Yarmouk University, 21163 Irbid, Jordan.

Abstract: Computational condensed matter physics is nowadays a highly developed field of research, in terms of basic theory, algorithms and applications. Providing a comprehensive account of this subject is hence far beyond the scope of any review article. Therefore, I will introduce this subject through a set of examples taken from my recent research work, which touch upon some important developments in this field. These developments are the exact exchange formalism within Kohn-Sham density functional theory, combined exact exchange and many-body quasiparticle approach (for highly accurate band structure calculations), and maximally localized Wannier functions. The theoretical background of the above approaches in addition to the density functional perturbation theory (used to calculate the phonon spectra and other related physical properties of solids) will be briefly described, and representative results are shown to demonstrate the accuracy and predictive power of these theoretical approaches.

I. Introduction

Direct application of standard quantum mechanics to condensed matter systems is a highly complicated many-body problem, which is simply impossible to solve both analytically or numerically. Thus, it is not surprising that in almost all practical quantum mechanical approaches the many-body problem is transformed to a single-body one. The magic of the Kohn-Sham (KS) formalism [1] of density functional theory (DFT) [2] arises from its proof that this transformation can be *exactly* performed. Thus, the problem of finding the system total energy, charge density and other ground state physical properties can be obtained by solving self-consistently a set of single-particle Schrödinger like equations (known as KS equations). The corresponding effective potential which is *functional* of the charge density, ρ, is called KS potential. In this formalism, all the quantum short-ranged effects are rolled up in the exchange-correlation (XC) energy term, $E_{XC}[\rho]$, which is the only part of the total energy that needs to be approximated. Moreover, the theory itself suggests some practical and well understood approximations for $E_{XC}[\rho]$. The most widely used are the local density approximation (LDA) and generalized gradient approximation (GGA). These approximations are found to give very good results for various properties of a wide range of materials, and this approach is currently being used to tackle fundamental problems in physics, chemistry, geophysics, material science and biology. See Ref. 3 for an excellent review of the basic theory and applications of this theoretical approach. A brief description of the KS-DFT formalism and E_{XC} is given in Sec. II.

Corresponding Author: Abdallah Qteish. **Email**: aqteish@yu.edu.jo

In spite of their enormous successes, the KS-DFT calculations have also several limitations. Here, we focus on two major sources of errors in the KS-DFT calculations based on LDA or GGA: (i) the presence of spurious self-interaction (SI) arising form the use of approximate exchange energy functionals [4], and (ii) the absence of a derivative discontinuity in the exchange-correlation potential with respect to changes in the particle number in both LDA and GGA functionals [5], which has a profound effect on the calculated band gaps of semiconductors and insulators. See Ref. [6] for a recent review of these limitations and their consequences, especially for transition metal and rare earth compounds. When applied to calculate the electronic structure of solids, two main problems are observed: (1) The band gap of semiconductors and insulators are highly underestimated (known as band gap problem), which is due to the above two deficiencies, and (2) the binding energies of the highly localized states are significantly lower than the corresponding experiment values, which is usually attributed to the spurious SI [7,8].

A recent important development is the exact exchange formalism within KS-DFT approach [9-11]. This is a major step forward, since the exchange energy is explicitly calculated, removing thus the spurious SI and leaving only the correlation energy to be approximated. It should be noted that the resulting *local* exact exchange potential is orbital dependent, which makes its computation very expensive in terms of both memory and CPU time, compared to LDA calculations. It has been recognized that this exact exchange potential is equivalent [12] to the optimized effective potential (OEP, Refs. 13 and 14): the best local potential that approximates the *non-local* Hartree-Fock potential, which has long been used in atomic and molecular calculations. Thus, this approach when used together with LDA correlation, hereafter denoted as OEPx(cLDA), is found to yield significant opening of the band gap of a wide range of semiconductors and insulators, leading to improved effective masses and optical properties [11]. However, the OEPx(cLDA) method does not completely solve the band gap problem, and we have shown [15] that

the removal of the SI, in this approach, does not improve the KS-DFT description of the binding energies of the highly localized states, contrary to the above common belief. The LDA, GGA and OEPx exchange-correlation functionals will be introduced in Sec. III.

For accurate band structure calculations, one thus needs to go beyond the KS-DFT formalism. The most widely used approach is the quasiparticle energy calculations [16,17] in Hedin's GW approximation [18] for the many-body self-energy operator. The application of the GW approximation to calculate the electronic structure of solids is pioneered by Hybertsen and Louie [19] and Godby, Schlüter and Sham [20]. The formal relationship between the quasiparticle energies and the experimental valence and conduction band energies, obtained respectively using photoemission spectroscopy and inverse photoemission spectroscopy, is clearly described in Ref. [17]. Originally, the Green's function G_0 and the screened potential W_0 required in the GW approximation (henceforth denoted G_0W_0) are calculated from a set of LDA single particle-energies and wave functions (LDA-G_0W_0). The LDA-G_0W_0 approach is found to accurately predict band gaps of *sp*-bonded semiconductors (with a typical error bar of 0.1 eV). However, complications arise when the LDA-G_0W_0 approach is used to calculate the electronic structure of semiconductors with negative LDA band gaps [21, 22] or when occupied shallow semicore *d* bands are treated as valence in the pseudopotential GW framework [23-25].

The above complications in the LDA-G_0W_0 calculations can be removed [17] by calculating G_0 and W_0 from OEPx(cLDA) single particle data [OEPx(cLDA)-G_0W_0]. This is another important development because of two reasons: (i) The quasiparticle corrections to the KS-DFT eigenvalues are commonly calculated by using first order perturbation theory. The opening of the band gaps within the OEPx(cLDA) makes these corrections smaller than those of LDA-G_0W_0, leading to a better validity and accuracy of these GW calculations. (ii) The OEPx(cLDA) method gives a much better description of the core states than LDA. This is especially important for the states whose wavefunctions

overlap strongly with those of the considered valence states, which allows the treatment of these highly localized states as part of the frozen core, contrary to the pseudopotential LDA-G_0W_0 approach [23-25]. Moreover, this also makes the generated OEPx(cLDA) pseudopotentials superior to those of LDA. We have found that the OEPx(cLDA)-G_0W_0 approach reproduces very well the band gaps of a wide range of semiconductors, including group-III nitrides [15,17,26-28], II-V compounds [17,29] and transition metal nitrides [30,31]. The OEPx(cLDA)-G_0W_0 approach will be introduced in Sec. IV.

Many physical properties of solids are directly related to successive derivatives of the system total energy with respect to external perturbations. These properties can be most efficiently calculated using density functional perturbation theory (DFPT); an interesting merging of perturbation theory and DFT [32-36]. This approach is based on a variational principle that provides accurate expressions for the energy derivatives and gives even access to non-linear responses. The perturbations considered in this review are the atomic displacements [35], homogeneous electric field [35] and homogeneous strain [37, 38]. Appropriate combinations of these perturbations give access to physical properties of primary interest: the dynamical matrices, elastic constants, Born effective charge and dielectric permittivity tensors. We have recently used this approach to investigate the elastic, dielectric, phonon spectra and thermal properties of some semiconductors [39-41]. The thermal properties of solids are usually studied by employing the quasiharmonic approximation [42,43]. However, very recently, the anharmonic effects have received renewed interest [44,45]. The calculations of these properties using DFPT will be described in Sec. V.

It is worth noting that the *ab inito* calculations of the phonon spectra have been started by Kunc and Martin [46], see also Ref. [47], using the so-called frozen-phonon approach. In this approach, the atoms are displaced according to a certain lattice vibrational mode, and the resulting lower symmetry structure is treated as a new crystal structure. Then, the phonon frequency of this mode is deduced from the difference in the total energy of the two structures (distorted and undistorted). A second technique is the interplanar force constant method [48]. In this approach, the force constants between the plans of atom normal to a high symmetry direction are determined by using the supercell method. A long enough unit cell is constructed along the considered high symmetry direction. The interplanar force constants are then extracted from the Hellmann-Feynman forces exerting on the atoms as a result of an appropriate displacement of central atom in an otherwise ground state structure (zero forces). This approach can be used to calculate the phonon modes along the high symmetry directions, and it is very useful in investigating the phonon dispersion relations of superlattices and heterostructures [49-51]. A third direct approach is the interatomic force constants (IFCs) method [52]. Here, the IFCs are calculated from the Hellmann-Feynman forces resulting from appropriate atomic displacements in a big enough supercell. This approach allows for the calculations of the phonon frequencies at a general k-point in the first Brillouin zone which, in turn, can be used to investigate the thermal properties of solids. On the other hand, the phonon frequencies and the free energy (including anharmonic effects) can be obtained using *ab initio* molecular dynamics, see for example Ref. [45]. However, the main disadvantage of the IFCs and molecular dynamic calculations lies in the relatively small size of the supercell considered. In the DFPT approach, on the other hand, the calculations are performed using the primitive unit cell.

Finally, the electronic states in a periodic potential can be described by either the widely used extended Bloch orbitals or in terms of localized Wannier functions (WFs). The non-uniqueness property of the WFs has dramatically limited their applications. An important recent development is the elegant method of Marzari and Vanderbilt [53] to construct unique maximally localized WFs (MLWFs). Hence, the WF representation has recently received considerable interest. In addition to their relevance in several areas of physics, WFs have found new interesting applications due to their connections with the Berry-phase theory of bulk polarization [54-56] and their potential use as basis in modern

electronic structure calculations to dramatically increase their efficiency [57,58]. We mention here the very recent highly efficient implementation of the GW calculations [58], in terms of MLWFs, which extends their applications to large systems (unit cells with hundreds of atoms). Other applications of the MLWFs include electrical and thermal transport [59,60], strongly correlated systems [61-63], photonic lattices [64], van der Waals interaction [65] and tight-binding calculations [66]. We have introduced [67] a novel first-principle bond ionicity scale based on the centers of the MLWFs. Concepts such as valency, electronegativity and bond ionicity are still very useful in understanding the differences in the properties of different systems and in seeking trends of these properties. Both the MLWFs and the new ionicity scale will be briefly described in Sec. VI.

II. The Kohn-Sham Formalism of Density Functional Theory and Exchange- Correlation Energy

Most of the modern electronic structure calculations are based on density functional theory (DFT), introduced by Hohenberg and Kohn [2]. The DFT states that the electronic charge density, ρ, is a basic quantity as the many-body wavefunctions. This is achieved by proving two theorems: (i) There is a one-to-one correspondence between ρ and the external potential, V_{ext}, up to an additive constant. The V_{ext} determines, in turn, the many-body wavefunctions from which all the physical properties of any electronic system can be extracted. Hence, the physical properties of any electronic system can be expressed as functionals of ρ. Of particular importance is the total energy, $E_{tot}[\rho]$. (ii) A variational principle: the ground state total energy is the global minimum of $E_{tot}[\rho]$, and the ρ that minimizes this functional is the ground state ρ. The main difficulty here is that an explicit expression for $E_{tot}[\rho]$ is unknown.

In a subsequent seminal paper, Kohn and Sham (KS) [1] have introduced the following highly intelligent separation of $E_{tot}[\rho]$:

$$E_{tot}[\rho] = T_o + E_{ext} + E_H + E_{XC}, \qquad (1)$$

where T_o is the kinetic energy of the system of *non*-interacting electrons; E_{ext} is the interaction energy between the electrons and the external potential; E_H is the classical electron – electron (e-e) interaction energy given as

$$E_H = \frac{1}{2} \iint \frac{p(r)p(r')}{|r-r'|} dr\, dr', \qquad (2)$$

and E_{XC} is the sum of the exchange (E_X) and correlation (E_C) energies. It is worth noting that the first three terms can be exactly calculated, leaving only the unknown or difficult to calculate term (E_{XC}) to be approximated. Moreover, the use of T_o instead of kinetic energy of the system of interacting electrons, T, allows for an *exact* transformation from the many-body to single-body problems [1]. Thus, the ground state E_{tot} and ρ can be determined by solving self-consistently a set of single particle Schrödinger like equations (note that atomic units are used)

$$\left[-\frac{\nabla^2}{2} + V_{ext}(\boldsymbol{r}) + V_H(\boldsymbol{r}) + V_{XC}(\boldsymbol{r}) \right] \phi_i(\boldsymbol{r}) = \varepsilon_i \phi_i(\boldsymbol{r}). \qquad (3)$$

Here, V_{ext}, V_H and V_{XC} are, respectively, the external potential, Hartree and XC potentials defined as

$$V_J(\boldsymbol{r}) = \frac{\delta E_J}{\delta \rho(\boldsymbol{r})} \qquad (4)$$

[with J stands for *ext*, *H* or *XC*].

The electron charge density distribution, ρ, is defined in terms of single-particle orbitals, ϕ_i, as

$$\rho(\boldsymbol{r}) = \sum_i f_i \left| \phi_i(\boldsymbol{r}) \right|^2, \qquad (5)$$

where f_i denotes the occupation number of the ith state. Eqs. (1) to (5) have to be solved self-consistently after an approximation for $E_{XC}[\rho]$ is adopted. Several practical methods are currently in use for such a purpose [3]. In our calculations, we employ a norm-conserving pseudopotential plane-wave method [68].

The $E_{XC}[\rho]$ part of the e-e interaction energy deserves a brief description. Let us connect first with the single-particle approach introduced by Hartree in 1930, in which V_{XC}

and E_{XC} are completely neglected from the above equations, and the many-body wavefunction of an N particle system is given as

$$\Psi(\boldsymbol{r}_1,\boldsymbol{r}_2,\boldsymbol{r}_3,...,\boldsymbol{r}_N) =$$
$$\psi_1(\boldsymbol{r}_1,\sigma_1)\psi_2(\boldsymbol{r}_2,\sigma_2)...\psi_N(\boldsymbol{r}_N,\sigma_N). \qquad (6)$$

Here, ψ_i is the product of the single particle spatial wavefunctions $\{\phi_i(\boldsymbol{r})\}$ and spin wavefunctions $\{\alpha_i(\sigma)\}$. This form of Ψ does not satisfy Pauli's exclusion principle, which requires anti-symmetric wavefunction. In the Hartree-Fock (HF) [69] approach, this principle is satisfied by writing Ψ as a Slater determinant

$$\Psi = \frac{1}{(N\,!)^{1/2}}$$
$$\times \begin{vmatrix} \psi_1(\boldsymbol{r}_1,\sigma_1) & \psi_1(\boldsymbol{r}_2,\sigma_2) & \psi_1(\boldsymbol{r}_3,\sigma_3) & ..... \\ \psi_2(\boldsymbol{r}_1,(\sigma_1) & \psi_2(\boldsymbol{r}_2,\sigma_2) & \psi_2(\boldsymbol{r}_3,\sigma_3) & ..... \\ . & . & . & ..... \\ . & . & . & ..... \end{vmatrix}.$$
$$(7)$$

This choice for Ψ leads to an additional orbital dependent exchange energy term

$$E_X = -\frac{1}{2}\sum_{i,j,\sigma}\int dr\,dr' \left(\phi_i^{\sigma*}(\boldsymbol{r})\phi_j^{\sigma*}(\boldsymbol{r}')\right.$$
$$\left.\times \frac{1}{|\boldsymbol{r}-\boldsymbol{r}'|}\phi_j^{\sigma}(\boldsymbol{r})\phi_i^{\sigma}(\boldsymbol{r}')\right). \qquad (8)$$

The corresponding exchange potential is non-local and orbital dependent, and the differential-integral equations to solve in the HF approach take the form

$$\int d^3\boldsymbol{x}' \left(\; -\frac{1}{2}\nabla^2\delta(\boldsymbol{x}-\boldsymbol{x}')+V_{ext}(\boldsymbol{x})\delta(\boldsymbol{x}-\boldsymbol{x}')\right.$$
$$+V_H(\boldsymbol{x})\delta(\boldsymbol{x}-\boldsymbol{x}')+V_X^{HF}(\boldsymbol{x},\boldsymbol{x}')\;\left)\phi_i(\boldsymbol{x}')\right.$$
$$=\sum_{i\neq j}\varepsilon_{ij}\phi_j(\boldsymbol{x}), \qquad (9)$$

with $\boldsymbol{x}$ here comprises the spatial coordinates $\boldsymbol{r}$ and spin σ. The HF exchange potential, $V_X^{HF}(\boldsymbol{x},\boldsymbol{x}')$, leads to the spatial separation between two electrons with equal spin. The exchange energy, E_X, is the reduction in the total energy resulting from the reduction of the Coulomb potential due to the above

spatial separation. Note that only semiconductors will be considered in this review, and all state summations, therefore, include the spin variable implicitly.

The correlation energy, E_C, is defined as the difference between the energy of the many-particle system and that calculated using the HF approach. It can be thought of as the further reduction in the total energy due the spatial separation of electrons with different spin. E_C is the most difficult term, and it is still an ongoing challenge in many-body theory.

III. Exchange - Correlation Functionals: LDA, GGA and Exact - Exchange

The DFT framework described in the previous section provides a practical tool for calculating the ground state properties of many-electron systems. This is largely due to the existence of accurate and well understood approximations for E_{XC}. The simplest and most widely used approximation is the LDA, proposed by Kohn and Sham [1]:

$$E_{XC}^{LDA}[\rho] = \int d\boldsymbol{r}\rho(\boldsymbol{r})\varepsilon_{XC}^{hom}(\rho(\boldsymbol{r})), \qquad (10)$$

where, ε_{XC}^{hom} is the XC energy per particle of a homogeneous electron gas of density $\rho(\boldsymbol{r})$, which is known with a very high accuracy. Although it is supposed to be valid for slowly varying $\rho(\boldsymbol{r})$, LDA is proved to be remarkably successful for various properties of a wide range of systems. The reasons behind the success of LDA are thoroughly investigated [70]. However, it has several drawbacks. For solids, the general understanding is that LDA slightly underestimates the lattice parameter and overestimates the cohesive energy and bulk modulus. However, as noted in the introduction, the most serious shortcoming is the so-called band-gap problem.

The other widely used approximation is the generalized gradient approximation (GGA), where information about the local variation of $\rho(\boldsymbol{r})$ is taken into account:

$$E_{XC}^{GGA}[\rho] = \int d\boldsymbol{r}\rho(\boldsymbol{r})\varepsilon(\rho(\boldsymbol{r}),|\nabla\rho(\boldsymbol{r})|) . \qquad (11)$$

Several GGA functionals have been devised, which try to satisfy as much as possible the properties and scaling rules of the exact E_{XC}

[71]. The main success of the GGA is a definite improvement in the cohesive energy of solids and molecules. Its performance for other properties, such as lattice parameter and bulk modulus of solids, is not impressive: the GGA results may even be worse than the LDA ones. As for the electronic structure, the differences between those calculated using LDA and GGA are marginal.

In principle, DFT is self-interaction free: for each electron the self-exchange energy [i.e, $i = j$ in Eq. (8)] cancels completely its self-Hartree one [Eq. (2), with $\rho_i(r)$ is used instead of $\rho(r)$]. Such a cancellation becomes incomplete when an approximation for E_X is adopted (while treating E_H exactly), leading to a spurious SI that is positive in nature [4]. The SI increases with the increase of the degree of localization of the electronic states. For example, the LDA eigenvalue of the $1s$ state of the H atom is about one half of the true value of 1 Ryd. Several methods have been introduced to remove or reduce the SI: (i) The self-interaction corrected LDA (SIC-LDA) of Perdew and Zunger [4] and its subsequent variants [7, 8, 72-74]. This is simply done by subtracting the interaction of each electron with its own charge density from the LDA (or the local spin-density (LSD) approximation) total energy. (ii) The LDA+U method [75], where the adjustable state dependent Hubbard U parameter is added locally to reduce the energies of the highly localized states. (iii) The use of hybrid functionals [76], which approximates the exchange potential as a linear combination of the corresponding non-local HF and local GGA potentials. (iv) The exact-exchange scheme within the KS-DFT method [9-11], which is practically SI free.

In the exact-exchange formalism within KS-DFT, E_X is calculated explicitly according to Eq. (8). The major difficulty here lies in the orbital dependence of E_X: note that V_X is defined as the first order variation of E_X with respect to $\rho(r)$, Eq. (4). This difficulty can be solved by using the chain rule:

$$V_X^{OEP}(\mathbf{r}) = \frac{\delta E_X}{\delta \rho(\mathbf{r})} =$$

$$\sum_i \iint \left[\frac{\delta E_X[\rho]}{\delta \varphi_i(r')} \frac{\delta \varphi_i(r')}{\delta V^{KS}(r'')} + c.c. \right] \frac{\delta V^{KS}(r'')}{\delta \rho(\mathbf{r})}. \quad (12)$$

As noted in Sec. I, this local exchange potential is equivalent to the optimized effective potential (OEP): the best local approximation to the HF non-local exchange potential [77]. The first derivative of Eq. (12) can be directly obtained from Eq. (8); the second derivative can be calculated using first order perturbation theory, while the third derivative is nothing but the inverse of the independent particle susceptibility,

$$\chi_o(\mathbf{r}, \mathbf{r}') = \delta \rho(\mathbf{r}) / \delta V^{KS}(\mathbf{r}'). \quad (13)$$

See Ref. 11 for other technical details. We note here that the calculation of V_X^{OEP} is quite involved and expensive in terms of both CPU time and memory, compared to LDA. More
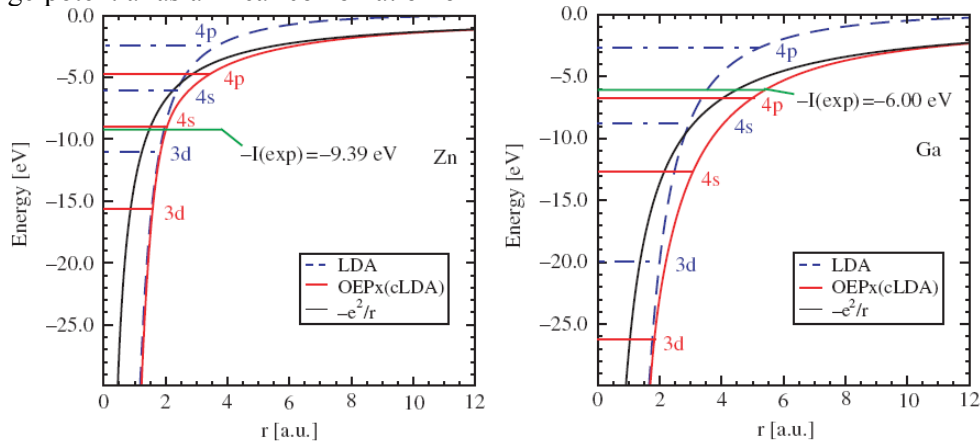
FIG.1. Effective Kohn–Sham potential for the neutral Zn (left panel) and Ga (right panel) atom: the OEPx(cLDA) potential (red line) reproduces the correct asymptotic decay$-e^2/r$ (black line), whereas the LDA (blue, dashed line) decays exponentially and thus underbinds the electrons. The atomic levels (shown as horizontal lines) are lowered in the OEPx(cLDA) approach compared to the LDA, resulting in good agreement with the experimentally measured ionization potential (green horizontal line). (Taken from Ref. 17).

efficient methods for calculating V_X^{OEP} have been recently introduced [78, 58].

The advantages of using the OEPx approach can be easily inferred from Fig. 1. First, the removal of the SI by this approach gives the correct asymptotic $-e^2/r$ behavior at large r. It is worth noting that, in this limit, the Coulomb potential of neutral atoms goes to zero, and the XC hole (which satisfies the sum rule: the XC hole density integrates to minus one electron) potential leads to the above asymptotic behavior. On the other hand, the LDA and GGA potentials go very rapidly to zero. Second, the removal of the SI by the OEOx(cLDA) approach improves

dramatically the calculated valence eigenvalues. The difference between the LDA (blue lines) and OEOx(cLDA) (red lines) eigenvalues is due to the SI. The OEOx(cLDA) value of the highest valence state energy is very close to the negative of the experimental ionization energy, as expected. Third, The deeper OEOx(cLDA) potential increases the spatial localization of the valence states, compared to those of LDA, leading to a smaller overlap between them in the formation of solids. This leads, in turn, to larger band gaps and smaller band widths relative to those of LDA. This is shown in Fig. 2 for the band gaps of several semiconductors.
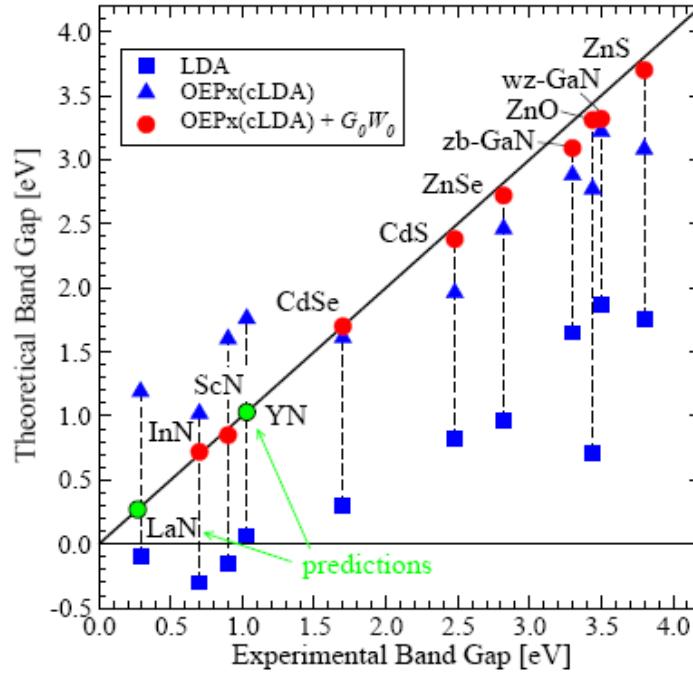
FIG. 2. Calculated *versus* experimental band gaps for selected II-VI compounds, group-III-nitrides and transition metal nitrides. The OEPx(cLDA)-G_0W_0 method consistently improves over LDA and OEPx(cLDA). For lack of experimental information on the band gap of YN and LaN, our predicted gaps have been placed on the diagonal. (Taken from Ref. 31).

IV. Quasiparticle GW Approach Based on Exact-Exchange KS-DFT Calculations

Via the field operator formalism, the many-body Hamiltonian can be transformed into a single-particle Hamiltonian [79]: $\hat{H}(\boldsymbol{r},\boldsymbol{r'};\varepsilon) = \hat{h}_o(\boldsymbol{r}) + \Sigma(\boldsymbol{r},\boldsymbol{r'};\varepsilon)$. All electron-electron interaction terms are rolled up in the non-local, energy-dependent self-

energy operator (Σ) and the remaining contributions are given by $\hat{h}_o(\boldsymbol{r}) = \frac{1}{2}\nabla^2 + V_{ext}(\boldsymbol{r})$. The single particle Green's function

$$G(\boldsymbol{r},\boldsymbol{r'};\varepsilon) =$$

$$\lim_{\eta \to 0^+} \sum_s \frac{\psi_s(\boldsymbol{r}),\psi_s^*(\boldsymbol{r'})}{\varepsilon - (\varepsilon_s + i\eta \operatorname{sgn}(E_f - \varepsilon_s))} \quad (14)$$

(where η is an infinitesimal positive energy) satisfies then the Dyson equation

$$G^{-1}(r,r';\varepsilon) = \left[\varepsilon - \hat{h}_0(r)\right]\delta((r-r') - \Sigma(r,r';\varepsilon). \tag{15}$$

By inserting Eq. (14) into (15), one immediately finds that ε_s and $\psi_s(\mathbf{r})$ are solutions to

$$\hat{h}_0(r)\psi_s(r) + \int dr'\Sigma(r,r';\varepsilon_s)\psi_s(r') \\ = \varepsilon_s\psi_s(r). \tag{16}$$

The poles of the Green's function therefore correspond to the real electron addition and removal energies ε_s and form a branch-cut infinitesimally above (below) the real energy axis for occupied (unoccupied) states.

To establish a link to photoemission of delocalized valence states, it is helpful to introduce Landau's concept of quasi-particles [80]. This new entity can be considered as a combination of an electron or a hole with its surrounding polarization cloud or, in other words, as the collective response of the interacting many-body system upon photoexcitation. Switching to the quasiparticle picture is consistent with analytically continuing the self-energy to the complex energy domain. Each of the quasi-particle poles (now at complex energy) represents the effect of many of the infinitesimally closely spaced poles just above (below) the real axis.

To solve the Dyson equation [Eq. (15)] for real systems, one typically applies Hedin's GW approximation [18] for the self-energy. Assuming that the quasi-particles interact only weakly via the screened Coulomb interaction W, the self-energy in the GW approach is then given as

$$\Sigma_{XC}^{GW}(r,r';\varepsilon) = \\ \frac{i}{2\pi}\int_{-\infty}^{\infty} d\varepsilon' e^{i\varepsilon'\delta}G(r,r';\varepsilon+\varepsilon')W(r,r';\varepsilon'), \tag{17}$$

where δ is an infinitesimal positive time. In practice, one starts from a system of non-interacting particles with energies ε_i and wavefunctions $\varphi_i(\mathbf{r})$. The non-interacting Green's function is defined analogous to Eq. (14) as

$$G_0(r,r';\varepsilon) = \\ \mathop{Lim}_{\eta\to 0^+}\sum_i \frac{\phi_i(r),\phi_i^*(r')}{\varepsilon - (\varepsilon_i + i\eta\,\mathrm{sgn}(E_f - \varepsilon_i))}. \tag{18}$$

The quantum state indices i and s are short for the composite of band index n and wave vector $\mathbf{k}$. In the random-phase approximation, the dielectric function,

$$\varepsilon(r,r';\varepsilon) = \\ \delta(r-r') - \int dr''V(r-r'')\chi_0(r,r';\varepsilon) \tag{19}$$

is connected to the independent-particle polarizability,

$$\chi_0(r,r';\varepsilon) = \\ -\frac{i}{2\pi}\int_{-\infty}^{+\infty} d\varepsilon''G_0(r,r'';\varepsilon'-\varepsilon)G_0(r,r'';\varepsilon')\chi_0 - r''$$

$$\tag{20}$$

and the bare Coulomb interaction,

$$V(r-r') = \frac{1}{|r-r'|}, \tag{21}$$

is screened by the inverse dielectric function

$$W_0(r,r';\varepsilon) = \int dr''\varepsilon^{-1}(r,r'';\varepsilon)V(r''-r). \tag{22}$$

Separating the Hartree potential from the GW self-energy, and inserting Σ_{XC}^{GW} and the quasi-particle Green's function [Eq. (14)] into Eq. (15), the Dyson equation becomes

$$\left[\hat{h}_0(r) + V_H(r)\right]\psi_s(r) \\ + \int dr'\Sigma_{XC}^{GW}(r,r';\varepsilon_s)\psi_s(r') = \varepsilon_s\psi_s(r) \tag{23}$$

This equation, also referred to as quasi-particle equation, can be solved for the quasi-particle energies and wavefunctions.

Most commonly, the quasiparticle energies $\{\varepsilon_s^{qp}\}$ are determined using first order perturbation theory

$$\varepsilon_{nk}^{qp} = \varepsilon_{nk}^{DFT} \\ + <\phi_{nk}|\Sigma_{XC}^{G_0W_0}(\varepsilon_{nk}^{DFT}) - V_{XC} - \Delta\mu|\phi_{nk}>. \tag{24}$$

Here, G_0 and W_0 used to calculate $\Sigma_{XC}^{G_0W_0}$ are computed from a set of KS-DFT single-particle-energies and wave functions $\{\varepsilon_i^{DFT}, \phi_i^{DFT}\}$, and the constant $\Delta\mu$ is

introduced to align the Fermi energies before and after applying the GW self-energy corrections. Since G_0 and W_0 are not usually updated in a self-consistent manner, the so-calculated quasiparticle energies depend on the XC approximation used to calculate the input data. In the LDA-G_0W_0 approach, G_0 and W_0 are calculated from LDA data, while OEPx(cLDA) data are used in the OEPx(cLDA)-G_0W_0 method. As previously noted, the LDA-G_0W_0 results were found to accurately predict band gaps of sp-bonded semiconductors (with a typical error bar of 0.1 eV) [81]. However, complications arise when the LDA-G_0W_0 approach is used to calculate the electronic structure of semiconductors with *negative* LDA band gaps [21, 22] or when occupied shallow semicore d bands are treated as valence in the pseudopotential LDA-G_0W_0 framework [23-25]. We have found that OEPx(cLDA)-G_0W_0 method provides a reliable tool for band structure calculations of a wide range of semiconductors, including group-III nitrides [15, 17, 26-28], II-VI compounds [17, 29] and transition metal nitrides [30, 31], as shown in Fig. 2 and Table I.

Table I shows that the quasiparticle band gaps calculated using the OEPx(cLDA)-G_0W_0 approach are much superior than those of LDA-G_0W_0. This can be understood as

TABLE I. DFT and quasiparticle band gaps in eV for ZnO, ZnS, CdS and GaN in the zinc-blende structure compared to the experimental values. The calculations are performed using a pseudopotential plane-wave approach, with the semicore d electrons treated as valence. LDA calculations highly underestimate the band gap. The situation is improved by the quasiparticle LDA-G_0W_0 calculation, but the band gaps are still much smaller than the experimental values (see text). The OEPx(cLDA) approach leads to a significant opening of the band gap (relative to those of LDA), and OEPx(cLDA)-G_0W_0 results are in excellent agreement with experiment. (Taken from Ref. 29).

Method	ZnO	ZnS	CdS	GaN
LDA	0.51	1.76	0.81	1.65
LDA-G_0W_0	1.36	2.59	1.60	2.54
OEPx(cLDA)	2.34	2.94	1.84	2.76
OEPx(cLDA)-G_0W_0	3.11	3.70	2.39	3.09
Experiment	3.44	3.80	2.48	3.30

follows. It has been argued that wavefunctions of the semicore d electrons in the considered systems overlap strongly with those of the s and p electrons of the same shell. To obtain accurate quasiparticle band gaps within the pseudopotential LDA-G_0W_0 approach, the *entire* semicore shell should be included as part of the valence states [23-25], which makes these calculations highly expensive. Including instead only the semicore d electrons as valence results in large errors in the calculated band gaps, as is evident from Table I. On the other hand, these semicore s and p states are well described by the OEPx(cLDA) scheme, and hence they can be kept as part of the frozen core in the pseudopotential OEPx(cLDA)-G_0W_0 calculations. The other main advantage of the OEPx(cLDA)-G_0W_0 approach is the significant opening of the band gap arising from the removal of the self-interaction, compared to those of LDA, see above. This means that $V_{XC}^{OEPx(cLDA)}$ is closer to the self-energy operator Σ_{XC}^{GW} than V_{XC}^{LDA}, which leads to a better validity of the first order perturbation theory [Eq. (24)] used to calculate the quasiparticle energies.

As an example, we focus here on the band gap (E_g) of wurtzite (wz) InN. Experimentally, the widely accepted band gap (of 1.9 eV) has been recently questioned [82-84], and a value of about 0.7 eV has been measured in new high quality samples (low carrier concentration resulting from n-type doping). Moreover, the conduction electrons effective mass (m^*) of wz-InN is also found to depend strongly on the carrier concentration in the sample [27].

We show in Fig. 3 the calculated band structure of wz-InN in the vicinity of the band gap. The LDA calculations give incorrectly a negative band gap at the Γ point, which makes problematic the application of the LDA)-G_0W_0 method to this system [21,22]. On the other hand, the OEPx(cLDA) approach leads to sizable opening of the band gap, making wz-InN correctly a direct band gap semiconductor. The opening of the band gap in the latter approach is a direct consequence of the removal of the self-interaction: the energy of the relatively more localized upper valence states is lowered more than that of the lower conduction band
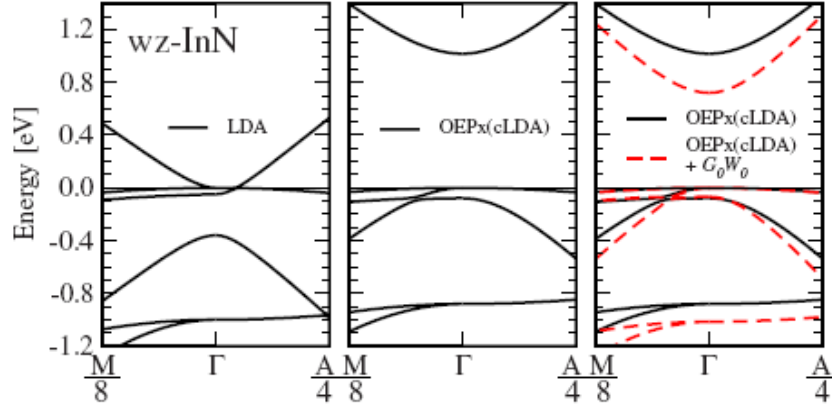
FIG. 3. LDA Kohn-Sham calculations incorrectly predict wurtzite InN to be a metal with the wrong band ordering at the Γ point. In OEPx(cLDA), the band gap opens and InN correctly becomes a semiconductor, thus providing a more suitable starting point for subsequent quasiparticle energy calculations in the G_0W_0 approximation. (Taken from Ref. 27).
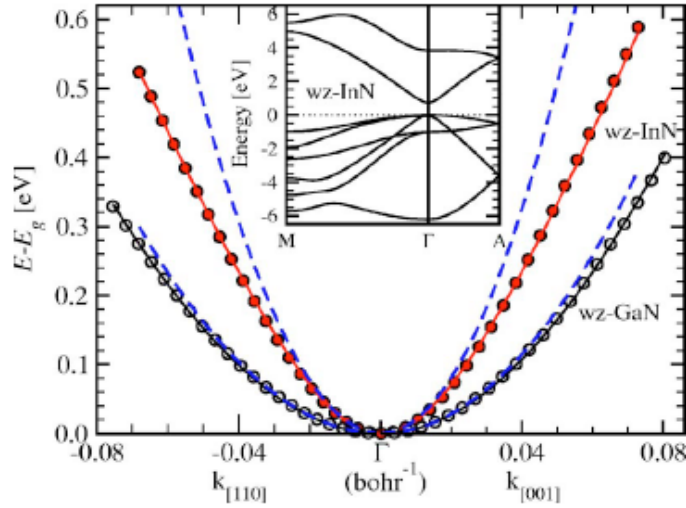
FIG. 4. Conduction band of wurtzite InN and GaN aligned at the bottom of the conduction band: the circles are the OEPx(cLDA)-G_0W_0 results, the solid lines the $\mathbf{k} \cdot \mathbf{p}$ fit using Eq. (25), and the dashed lines the effective mass band (i.e, parabolic shape). The inset shows the band structure of wurtzite InN. (Taken from Ref. 27).

states. Finally, the quasiparticle correction to the OEPx(cLDA) band gap (using the OEPx(cLDA)-G_0W_0 scheme) leads to a band gap that is in excellent agreement with the recent experimental results [82-86].

To explain the sizable dependence of the band gap and conduction electrons effective mass of wz-InN on the carrier concentration (n-type), we use an analytic expression for the conduction band around the Γ point

$$E_c(k) = \frac{\hbar^2 k^2}{2m_o} + \frac{1}{2}\left(E_g^+ + \sqrt{(E_g^-)^2 + 4E_p \frac{\hbar^2 k^2}{2m_o}} \right) \quad (25)$$

derived from a four band $\mathbf{k} \cdot \mathbf{p}$ model, neglecting spin-orbit splitting. Here, m_o is the free electron mass and $E_g^{\pm} = E_g \pm \Delta_1$, where Δ_1 is the crystal field splitting parameter of the upper three valence band states at the Γ point. The parameter E_p is related to the optical matrix elements between conduction and valence bands. Since it is the only unknown in Eq. (25), it has been determined by fitting to the OEPx(cLDA)-G_0W_0 conduction band. The calculated and fitted conduction bands around the Γ point are shown in Fig. 4, for wz-InN and wz-GaN. Using the OEPx(cLDA)-G_0W_0 values for Δ_1 and E_g, we find that the quasiparticle

140

conduction band of InN is well described by E_p of 9.0 eV (red solid line in Fig. 4).

Let us start first with the conduction electrons effective mass, m^*. In the spherical band approximation, the momentum effective mass

$$\frac{m^*(k_F)}{m_0} = \left(\frac{m_0}{\hbar^2 k_F} \frac{dE_c(k)}{dk} \bigg|_{k=k_F} \right)^{-1} \qquad (26)$$

can be translated into a carrier concentration dependent effective mass using the free electron relation $k_F = (3\pi^2 \rho)^{1/3}$, where ρ is the density of electrons in the conduction band. Fig. 5 shows the effective mass of wz-InN as a function of the free carrier concentration. The *ab initio* prediction (red line) extracted from our OEPx(cLDA)-G_0W_0 band structure by means of Eqs. (25) and (26) reproduces the experimental results very well and closely matches the curve obtained by Wu *et al.* with an experimentally deduced value of E_p =10 eV [Refs. 85 and 86 (black line)].

The n-type doping has also a direct consequence on the direct optical transitions $[E_g(\rho) = E_c(\rho) - E_v(\rho)]$ of wz-InN, which are shifted towards higher energies due to conduction band filling as the free electron concentration increases — the so-called Burnstein-Moss effect. Contributions from the electron-ion and electron-electron repulsions at high electron concentrations are accounted for following Wu *et al.* [85, 86]. The Burnstein-Moss shift calculated in this way fits very well a wide range of experimentally reported measurements, as shown in Fig. 6, and agrees well with the curve deduced by Wu *et al.* from their experimentally determined values of E_g and E_p. Neglecting the non-parabolicity of the conduction band (blue dashed line) worsens the agreement with the experimental results.

The excellent agreement between the OEPx(cLDA)-G_0W_0 results and experiment for the band gap of a wide range of semiconductors (Fig. 2) and in the delicate case of wz-InN (Figs. 5 and 6) reflects the high accuracy and predictive power of this method. This approach is nowadays one of the most advanced methods for band structure calculations.
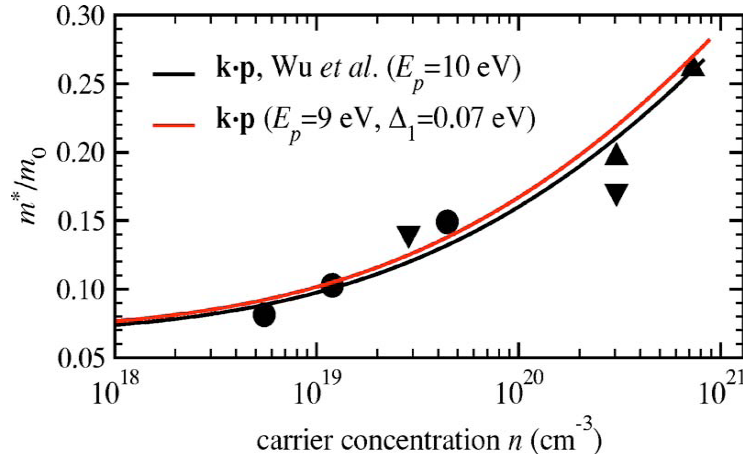
FIG. 5. The wz-InN effective mass as a function of carrier concentration, deduced from the OEPx(cLDA)-G_0W_0 calculations by means of Eqs. (25) and (26) [red line], agrees well with experimental measurements (symbols) and the **k·p** fit of Wu *et al.* (black line) based on the experimental data ([85, 86]). (Taken from Ref. 27).
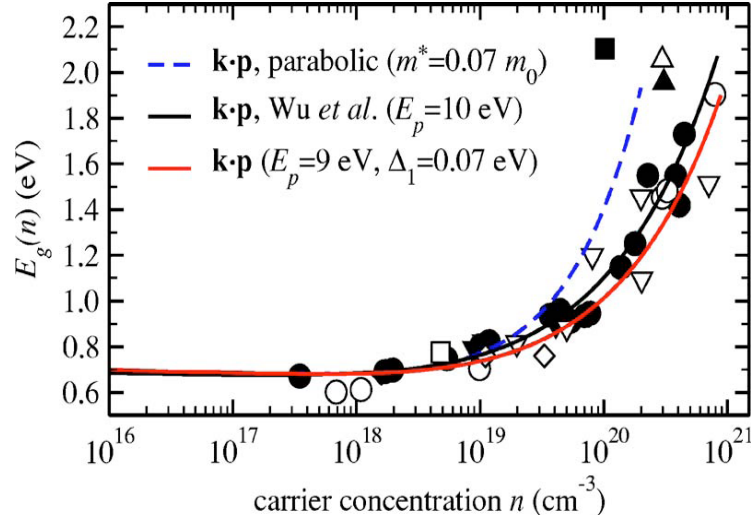
FIG. 6. Burnstein-Moss effect deduced from the OEPx(cLDA)-G_0W_0 band structure (red line) for wz-InN reproduces the experimental trend (symbols) very well and is also close to the **k·p** curve of Wu *et al.* (black line) [85, 86]. Assuming parabolic bands (dashed line) overestimates the Burnstein-Moss shift. (Taken from Ref. 27).

V. Elastic, Dielectric, Vibrational and Thermal Properties of Semiconductors from DFPT Calculations

Many properties of solids are defined as a response to an external perturbation. Here, we will focus on the perturbations that can be handled by the ABINIT computer package [87]: the atomic displacements ($\boldsymbol{u}_m$) that preserve the crystal periodicity, homogeneous electric fields (E_α, where α denotes a Cartesian direction) and homogeneous strains (η_j, where $j = \{1...6\}$ in Voigt notation). The corresponding responses that are conjugate to these perturbations are (i) forces $\boldsymbol{F}_m$, (ii) polarizations P_α and (iii) stresses σ_j, respectively. From a simultaneous application of a pair of these perturbations, one gets response functions of primary interest: $K_{mn} = d\boldsymbol{F}_m / d\boldsymbol{u}_n$ (interatomic force-constant matrix), $\varepsilon_{\alpha\beta} = P_\alpha / E_\beta$ (dielectric susceptibility), $C_{jk} = d\sigma_j / d\eta_k$ (elastic constants), $Z^*_{m\alpha} = dP_\alpha / du_m$ (Born effective charge), $\boldsymbol{\Lambda}_{mj} = d\boldsymbol{F}_m / d\eta_j$ (internal strain) and $e_{\alpha j} = dP_\alpha / d\eta_j$ (piezoelectric response). These response tensors are nothing but second order derivatives of the total energy with respect to appropriate mixed perturbations. These energy derivatives can be efficiently calculated, within DFPT, by a variational technique similar to the one usually adopted to solve the KS equations. The force-constant

matrices can then be used to find the phonon modes over the entire Brillouin zone, which are the basic ingredient needed to calculate the thermal properties of solids.

V.A. Density functional perturbation theory

In the usual formulation of DFPT, the dependence of the electronic part of the total energy (E_{el}) on a parameter λ is developed as a power series in λ [35]:

$$X(\lambda) = X^{(0)} + \lambda X^{(1)} + \lambda^2 X^{(2)} + ... \qquad (27)$$

This power series expansion applies to other exact perturbed physics quantities: $\{\varphi\}$, $\{\varepsilon\}$, ρ, V_{ext}, T_0, H, … etc. Now, the second order derivative of E_{el} (or $E_{el}^{(2)}$) is stationary relative to variations in the first order derivative of $\{\varphi\}$, thanks to the 2n+1 theorem [88], and is given as

$$\begin{aligned} E_{el}^2\{\varphi^{(0)}; \varphi^{(1)}\} = \sum_i^{occ} \Big[&< \varphi_i^{(1)} | (H^{(0)} - \varepsilon_i^{(0)}) | \varphi_i^{(1)} > \\ &+ (< \varphi_i^{(1)} | (T_0^{(1)} + V_{ext}^{(1)}) | \varphi_i^{(0)} > + \\ &< \varphi_i^{(0)} | (T_0^{(1)} + V_{ext}^{(1)}) | \varphi_i^{(1)} >) \\ &+ < \varphi_i^{(0)} | (T_0^{(2)} + V_{ext}^{(2)}) | \varphi_i^{(0)} > \qquad (28) \\ &+ \frac{1}{2} \iint \frac{\delta^2 E_{H,XC}}{\delta\rho(\boldsymbol{r})\delta\rho(\boldsymbol{r}')} \rho^{(1)}(\boldsymbol{r})\rho^{(1)}(\boldsymbol{r}')d\boldsymbol{r}d\boldsymbol{r}' \\ &+ \int \frac{\partial}{\partial\lambda} \frac{dE_{H,XC}}{\delta\rho(\boldsymbol{r})}\Big|_{\rho^{(0)}} \rho^{(1)}(\boldsymbol{r})d\boldsymbol{r} \\ &+ \frac{1}{2} \frac{\partial^2 E_{H,XC}}{\partial\lambda^2}\Big|_{\rho^{(0)}} \end{aligned}$$

142

where $E_{H,XC}$ is the sum of the Hartree and XC energies, and $\rho^{(I)}$ is given by

$$\rho^{(1)}(\boldsymbol{r}) = \sum_i^{occ} \left[\varphi_i^{*(1)}(\boldsymbol{r})\varphi_i^{(0)}(\boldsymbol{r}) + \varphi_i^{*(0)}(\boldsymbol{r})\varphi_i^{(1)}(\boldsymbol{r}) \right].$$
(29)

Since $\{\varphi^{(0)}\}$ are already known from self-consistent calculations of the unperturbed system, $E_{el}^{(2)}$ is functional of only $\{\varphi^{(1)}\}$. The variation of $\{\varphi^{(1)}\}$ to minimize $E_{el}^{(2)}$ should be done subject to the constraint

$$<\varphi_i^{(1)} \mid \varphi_j^{(0)} > = 0$$
(30)

for all the occupied states i and j. Under such constraint, $\{\varphi^{(1)}\}$ satisfy the self-consistent Sternheimer equation [89], which is the Euler-Lagrange equation for this functional,

$$P_c \left(H^{(0)} - \varepsilon_i^{(0)} \right) P_c \mid \varphi_i^{(1)} > = $$
$$- P_c H^{(1)} \mid \varphi_i^{(0)} >$$
(31)

where P_c is the projector onto unoccupied states (conduction bands states) and

$$H^{(1)} = T^{(1)} + V_{ext}^{(1)} + V_{H,XC}^{(1)}, \text{ with}$$

$$V_{H,XC}^{(1)} = V_{H,XC0}^{(1)} + \int \frac{\delta^2 E_{H,XC}}{\delta\rho(\boldsymbol{r})\delta\rho(\boldsymbol{r}')} \rho^{(1)}(\boldsymbol{r}')d\boldsymbol{r}',$$

and

$$V_{H,XC0}^{(1)} = \frac{\partial}{\partial\lambda} \left. \frac{\delta E_{H,XC}}{\delta\rho(r)} \right|_{\rho^{(0)}}.$$
(32)

Now, Eqs. (28) to (32) can be solved self-consistently, for example using the conjugate gradient technique, as nowadays usually done for solving the KS equations for $E_{el}^{(0)}$ and $\rho^{(0)}$ [Eqs. (1) to (5)].

The computation of response tensors described above involves mixed second derivatives of E_{el} with respect to two different perturbations, except the diagonal elements of the elastic tensor. In this case, Eq. (27) can be generalized as

$$E_{el}(\lambda_1,\lambda_2) = E_{el}^{(0)} + \lambda_1 E_{el}^{(\lambda_1)} + $$
$$\lambda_2 E_{el}^{(\lambda_2)} + \lambda_1\lambda_2 E_{el}^{(\lambda_1\lambda_2)} + \dots\dots$$
(33)

While stationary expressions for such mixed derivatives of E_{el} can be derived, they are usually calculated using the simpler nonstationary expression

$$E_{el}^{\lambda_1\lambda_2} = $$
$$\sum_i^{occ} \Big[< \varphi_i^{(\lambda_2)} \mid (T_0^{(\lambda_1)} + V_{ext}^{(\lambda_1)} + E_{H,XC}^{(\lambda_1)}) \mid \varphi_i^{(0)} >$$
$$+ (< \varphi_i^{(0)} \mid (T_0^{(\lambda_1\lambda_2)} + V_{ext}^{(\lambda_1\lambda_2)}) \mid \varphi_i^{(0)} >$$
$$+ \frac{1}{2} \frac{\partial^2 E_{H,XC}}{\partial\lambda_1\lambda_2} \Big|_{\rho^{(0)}},$$
(34)

which requires the first-order wave functions for only one of the perturbations and just the non-self-consistent Hamiltonian terms for the other.

In the following subsection, we will describe briefly only the case of periodicity-preserving atomic displacement perturbations, which are used to calculate the interatomic force constant matrices. For homogeneous electric field and strain perturbations, interested readers may consult the original papers [35] and [37], respectively.

V.B. Periodicity-Preserving Atomic Displacements Perturbations

We start by noting that the unperturbed V_{ext} of a crystalline solid is periodic: $V_{ext}^{(0)}(\boldsymbol{r}+\boldsymbol{R}_a,\boldsymbol{r}'+\boldsymbol{R}_a) = V_{ext}^{(0)}(\boldsymbol{r},\boldsymbol{r}')$, where $\boldsymbol{R}_a$ is a real space translation vector. To preserve this periodicity even for the perturbed potential, we consider a **q**-dependent perturbing potential operator of the form [35]

$$V_{ext,q}^{(!)}(\boldsymbol{r}+\boldsymbol{R}_a,\boldsymbol{r}'+\boldsymbol{R}_a) = e^{i\boldsymbol{q}\cdot\boldsymbol{R}_a} V_{ext}^{(1)}(\boldsymbol{r},\boldsymbol{r}'). \quad (35)$$

It should be noted that such a perturbing potential is non-Hermitian and should be always used in conjunction with its Hermitian conjugate counterpart, written as $V_{ext,-q}^{(!)}$ (since its wave vector is –**q**), as well as a complex expansion parameter λ, such that

$$V_{ext}(\lambda) = V_{ext}^{(0)} + (\lambda V_{ext,q}^{(1)} + \lambda^* V_{ext,-q}^{(1)})$$
$$+ (\lambda^2 V_{ext,q,q}^{(2)} + \lambda\lambda^* V_{ext,q,-q}^{(2)}$$
$$+ \lambda^*\lambda V_{ext,-q,q}^{(2)} + \lambda^{*2} V_{ext,-q,-q}^{(2)}) + \dots$$
(36)

and a similar form applies for $E_{el}(\lambda)$:

$$E_{el}(\lambda) = E_{ext}^{(0)} + (\lambda E_{el,q}^{(1)} + \lambda^* E_{el,-q}^{(1)})$$
$$+ (\lambda^2 E_{el,q,q}^{(2)} + \lambda \lambda^* E_{el,q,-q}^{(2)} \qquad (37)$$
$$+ \lambda^* \lambda E_{el,-q,q}^{(2)} + \lambda^{*2} E_{el,-q,-q}^{(2)}) + \ \dots$$

Now, when q is not a vector of the reciprocal lattice, the requirement of invariance under translation of the whole system leads to [35]

$$E_{el,q}^{(1)} = E_{el,-q}^{(1)} = 0 \quad , \qquad (38)$$

and when $2q$ is not a vector of the reciprocal lattice, one gets

$$E_{el,q,q}^{(2)} = E_{el,-q,-q}^{(2)} = 0 \quad . \qquad (39)$$

Thanks to these equations, it can be shown that $E_{el,q,-q}^{(2)}$ is a real quantity, variational with respect to $\{\varphi^{(1)}\}$. Thus, $E_{el,q,-q}^{(2)}$ is calculated by applying the minimization technique of the preceding section, see Ref. 35 for further details.

V.C. Dynamical Matrix and Phonon Frequencies

To construct the dynamical matrix, one considers unit displacements of atoms in sublattice κ, along the α axis, multiplied by the infinitesimal λ (eventually, a complex quantity) and by a phase varying with the cell to which the atoms belong; the α component of their vector position is changed from $\tau_{\kappa,\alpha} + R_{\kappa,\alpha}$ to $\tau_{\kappa,\alpha} + R_{\kappa,\alpha} + \lambda e^{iq.R_a}$, with q wave vectors restricted inside the Brillouin zone. Atoms in the other sublattices are not displaced. These collective displacements are consistent with the one considered above [Eq. (35)], and hence preserve the periodicity of the unperturbed potential. For such displacements, expressions for the first and second order changes in V_{ext} are given in Ref. 35 and then used to evaluate the second order changes of E_{el} for such perturbations, $E_{el,-q,q}^{\tau_{\kappa\alpha}^* \tau_{\kappa'\beta}}$, as described above. Finally, the second order changes of ion-ion energy are added to $E_{el,-q,q}^{\tau_{\kappa\alpha}^* \tau_{\kappa'\beta}}$ to find the corresponding changes of the total energy, $E_{tot,-q,q}^{\tau_{\kappa\alpha}^* \tau_{\kappa'\beta}}$, which are the main ingredient of the dynamic matrix as we will show below.

On the other hand, the total energy of a periodic crystal with small lattice distortions from the equilibrium positions can be expressed as

$$E_{tot}(\{\Delta\tau\}) = E_{tot}^{(0)} +$$
$$\sum_{a\kappa\alpha}\sum_{b\kappa'\beta}\frac{1}{2}\left(\frac{\partial^2 E_{tot}}{\partial\tau_{\kappa\alpha}^a \partial\tau_{\kappa'\beta}^b}\right)\Delta\tau_{\kappa\alpha}^a \Delta\tau_{\kappa'\beta}^b + ..., \qquad (40)$$

where $\Delta\tau_{\kappa\alpha}^a$ is the displacement along direction α of the atom κ in the cell labeled a (with vector R_a), from its equilibrium position τ_κ^a.

The matrix of the interatomic force constants (IFCs) is defined as

$$K_{\kappa\alpha,\kappa'\beta}(a,b) = \left(\frac{\partial^2 E_{tot}}{\partial\tau_{\kappa\alpha}^a \partial\tau_{\kappa'\beta}^b}\right) \qquad (41)$$

and its Fourier transform is

$$\tilde{K}_{\kappa\alpha,\kappa'\beta}(q) = \frac{1}{N}\sum_{ab} K_{\kappa\alpha,\kappa'\beta}(a,b)e^{-iq.(R_a - R_b)}$$
$$= \sum_b K_{\kappa\alpha,\kappa'\beta}(,b)e^{iq.R_b} \qquad (42)$$

where N is the number of cells of the crystal. It should be noted that $\tilde{K}_{\kappa\alpha,\kappa'\beta}(q)$ is connected to the second-order derivative of the total energy with respect to collective atomic displacements

$$\tilde{K}_{\kappa\alpha,\kappa'\beta}(q) = 2E_{tot,-q,q}^{\kappa\alpha,\kappa'\beta} \qquad (43)$$

and it is the main ingredient of the dynamical matrix

$$\tilde{D}_{\kappa\alpha,\kappa'\beta}(q) = \tilde{K}_{\kappa\alpha,\kappa'\beta}(q)/(M_\kappa M_{\kappa'})^{1/2} \quad (44)$$

where M_κ is the mass of the κth atom.

The vibration frequencies $[e_\kappa(q|j)]$ and polarization vectors of the phonon modes with wave vector q are determined by solving the eigenvalue matrix equation

$$\sum_{\kappa'\beta}\tilde{D}_{\kappa\alpha\kappa'\beta}(q)e_{\kappa'\beta}(q|j) = \omega_{q,j}^2 e_{\kappa\alpha}(q|j). \qquad (45)$$

For polar compounds, the macroscopic electric field, caused by the long-range character of the Coulomb forces, contributes to the longitudinal optical phonons in the long wavelength ($q{\to}0$) limit. This effect is

included by calculating the nonanalytical part ($\widetilde{K}^{\text{na}}$) of the force constants, given by [35]

$$\tilde{K}^{na}_{\kappa\alpha\kappa'\beta} = \frac{4\pi e^2}{\Omega_0} \frac{\sum_{\beta'}(Z^*_{\kappa,\beta',\alpha}q_{\beta'})\sum_{\alpha'}(Z^*_{\kappa,\alpha',\beta}q_{\alpha'})}{\sum_{\alpha'\beta'}q_{\alpha'}\varepsilon_{\infty\alpha',\beta'}q_{\beta'}} \quad (46)$$

where, Z^* and ε_∞ are, respectively, the Born effective charges and the macroscopic high-frequency static dielectric tensors (see above) which are also calculated self-consistently using DFPT.

For a *nonpolar* material, the dynamical matrix is analytic in reciprocal space and the real space IFCs are quite short ranged (i.e., negligible beyond a certain range $R_{\max}$). In this case, the IFCs can be obtained by Fourier transformation of $\widetilde{K}_{\kappa\alpha,\kappa'\beta}(\boldsymbol{q})$ computed on a regular discrete mesh in $\boldsymbol{q}$ space of spacing $\Delta q \leq 2\pi / R_{\max}$. The so obtained IFCs can be used to compute the dynamical matrices at any arbitrary $\boldsymbol{q}$ point (i.e., a point not contained in the original grid). In case of a polar material, the dynamical matrix displays a nonanalytic behavior in the $\boldsymbol{q}\to 0$ limit, see above. Therefore, the nonanalytic contribution [Eq. (46)] is subtracted from the $\tilde{K}_{\kappa\alpha,\kappa'\beta}(\boldsymbol{q})$ at each $\boldsymbol{q}$ point in the grid. Fourier transforming these modified $\widetilde{K}_{\kappa\alpha,\kappa'\beta}(\boldsymbol{q})$ gives the short-ranged IFCs.

We have used DFPT to investigate the phonon spectra of several semiconductors [39-41] under zero and high pressures. As an example, we will focus here on those of ZnSe (a wide band gap semiconductor) [40]. Fig. 7 depicts the phonon spectra of ZnSe at zero and 9 GPa pressures. The most important feature to note here is the excellent agreement with experiment. The pressure variation of phonon spectra of ZnSe depicted by the mode Grüneisen parameter of ZnSe, defined as $\gamma_{j,q} = -(d\ln\omega_{j,q}(V)/d\ln V)$, is shown in Fig. 8. This figure shows that the optical and longitudinal acoustical (LA) branches are shifted up in frequency while the transverse acoustical (TA) branches experience a downward shift. We will show below that such a behavior has a direct impact on the thermal properties of ZnSe, especially in the case of thermal expansion.

Also shown in Fig. 7 are the results obtained with the semicore 3*d* electrons of Zn treated as part of the frozen core and including the non-linear exchange-correlation corrections (NLCC) [91]. The relaxation of the semicore *d* electrons is clearly required for highly accurate theoretical determination of the phonon spectra of IIB-VI compounds. However, their effects are rather small, and hence these electrons can be treated as part of the frozen core for computing the phonon spectra of big systems (large unit cells) involving group-II elements.
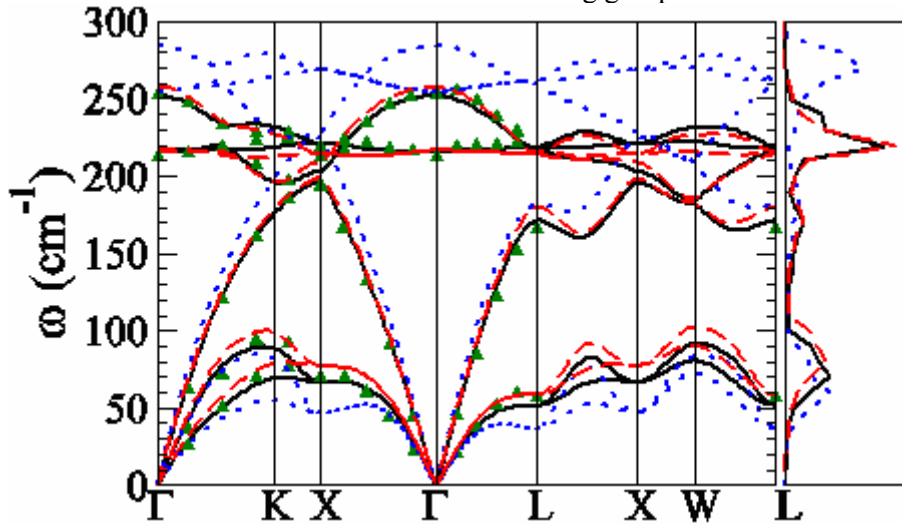
FIG. 7. Phonon spectra and density of states of ZnSe, at zero (solid lines) and 9 GPa (dotted lines) pressures. The calculated phonon spectra at zero pressure are in excellent agreement with the experimental data (triangles), obtained using inelastic neutron scattering [90]. NLCC calculations (see text) at zero pressure are shown with dashed lines. (Taken from Ref. 40).
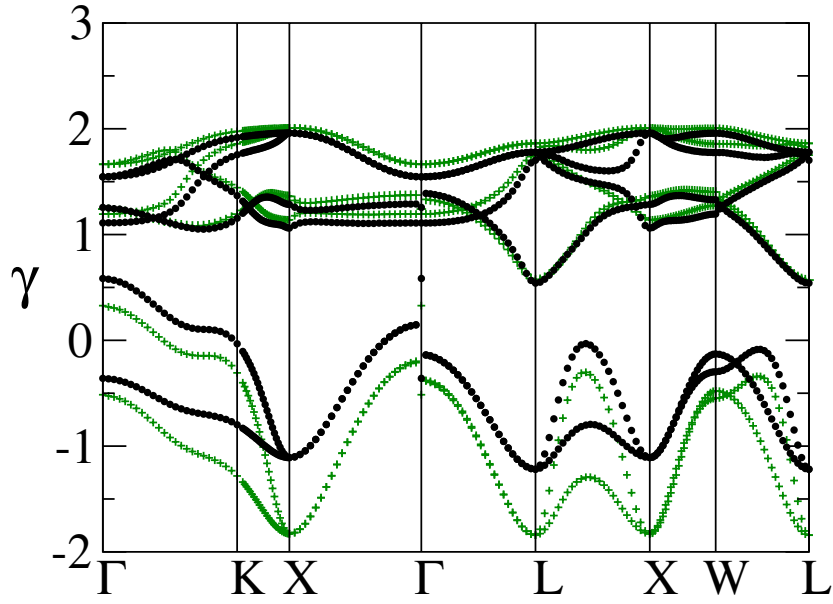
FIG. 8. Mode Grüneisen parameter of ZnSe, along several high symmetry directions of the fcc lattice, with (crosses) and without (circles) including the semicore $3d$ electrons of Zn as valence electrons. (Taken from Ref. 40).

For such a cubic material, the Born transverse effective charge tensor Z^* is isotropic. Because of the charge neutrality, the effective charge $Z^* = \mathrm{Tr}\, Z^*/3$ of the anions is minus that of the cations. The zero pressure value of Z^* of the cations of ZnSe is 2.026 (2.00) for $3d$ (NLCC) calculation, which is in excellent agreement with the experimental value of 2.03. On the other hand, the calculated zero pressure value of $\varepsilon_\infty = \mathrm{Tr}\, \varepsilon_\infty / 3$ of ZnSe is 7.53, which is considerably higher than the experimental value of 6.3. However, our NLCC value of 6.59 is in good agreement with the experiment and other similar theoretical results.

V.D. Equation of State, Thermal Expansion and Heat Capacity in the Quasiharmonic Approximation

The knowledge of the entire phonon spectrum of a given system enables the calculation of its thermodynamic properties and the relative stability of its different phases as functions of T. The thermodynamic properties are usually determined by the appropriate thermodynamic potential relevant to the given ensemble. In the ensemble where the sample volume (V) and T are independent variables, the relevant potential is the

Helmholtz free energy (F). In the adiabatic or Born-Oppenheimer approximation, F of a semiconductor can be written as

$$F = E_{tot} + F_{vib} = E_{tot} + E_{vib} - TS_{vib}, \qquad (47)$$

where E_{vib} and S_{vib} is the contribution of the lattice vibration to the internal energy and entropy (S), respectively. The electronic entropy contribution to S, vanishes identically for insulators, and thus, it is not included in Eq. (47). Even for metals, this contribution is usually neglected, although it is easy to calculate. Thus, the key quantity to calculate in order to have access to the thermal properties and to phase stability is F_{vib}.

F_{vib} is usually calculated within the quasiharmonic approximation (QHA). This means calculating F_{vib} in the harmonic approximation, retaining only the implicit V dependence through the phonon frequencies, and it is given as

$$F_{vib}(T,V) = k_B T \sum_{j,q} \ln(2\sinh(\hbar\omega_{j,q}(V)/2k_B T))$$

$$(48)$$

The QHA accounts only partially for the effects of anharmonicity. However, QHA is found to be a very good approximation at temperatures not too close to the melting point.

146
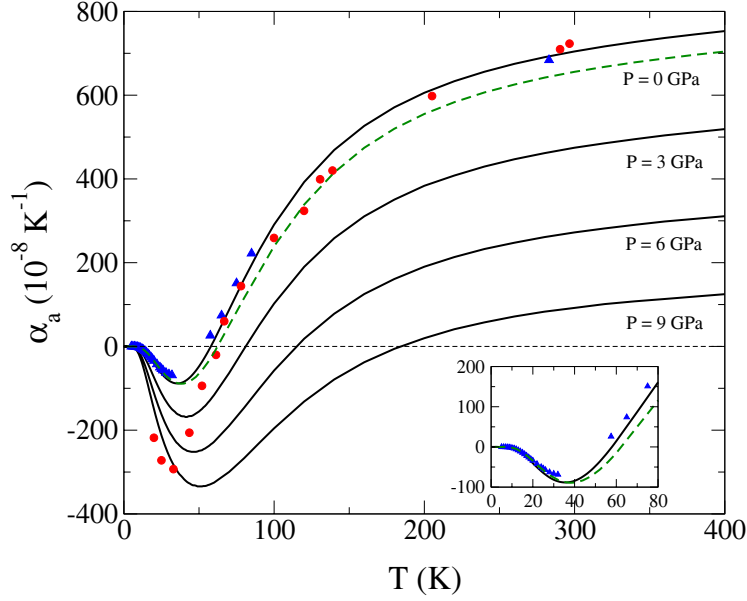
FIG. 9. Linear thermal expansion coefficient of ZnSe as a function of temperature, at different pressures. Solid lines: semicore 3d electrons treated as valence. Dashed line: NLCC calculations. At zero pressure, our results are in excellent agreement with the recent experimental results (Triangles: Ref. 94), which differ from previous experimental data (Circles: Ref. 95) at low temperatures. Inset: data in the temperature range of 0–80 K, at zero P. (Taken from Ref. 40).

For given T and V, the equilibrium state of a crystal is determined by minimizing F with respect to all possible degrees of freedom. The equation of state (P versus V) of the system is obtained by equating P to minus the derivative of F with respect to V at constant T, or

$$P = -(\partial F / \partial V)_T. \tag{49}$$

The thermal expansion can be directly obtained from the equation of state, and the volume thermal expansion coefficient is defined as

$$\alpha_V = \frac{1}{V}\left(\frac{\partial V}{\partial T}\right)_P. \tag{50}$$

The linear thermal expansion coefficient for cubic crystals is given as

$$\alpha_a = \frac{1}{3}\alpha_V. \tag{51}$$

Due to anharmonicity effects, the heat capacity at constant P (C_P) is different from that at constant volume (C_V). The former, which is what experiments directly determine, is proportional to T at high T, while the latter goes to a constant which is given by the classical equipartition law: $C_V =$ $3Nk_B$, where N is the number of atoms in the system. The relation between C_P and C_V is [92]

$$C_P - C_V = \alpha_V^2(T)B_0VT, \tag{52}$$

where B_0 is the bulk modulus. Within QHA, C_V is given as [88]

$$
C_V(T) = \\
\sum_{q,j} c_{q,j}^V(T) = \\
k_B \sum_{q,j}\left(\frac{\hbar\omega_{q,j}(V)}{2k_BT}\right)^2 \frac{1}{\sinh^2[\hbar\omega_{q,j}(V)/2k_BT]}, \tag{53}
$$

where $c_{q,j}^V(T)$ is the contribution to C_V of the j,$\mathbf{q}$ phonon mode at a certain T. The linear thermal expansion can be expressed in terms of $c_{q,j}^V(T)$ and $\gamma_{q,j}$ as [93]

$$\alpha_a(T) = \frac{1}{3B_0V}\sum_{q,j}\gamma_{q,j}c_{q,j}^V(T). \tag{54}$$

We have calculated the thermal properties of some semiconductors [40, 41], under zero and high pressures, at the level of LDA. As an example, we show in Figs. 9 and 10 the thermal expansion and heat capacity of ZnSe [40], respectively. The success of LDA in

147

describing such properties is clearly evident. The most interesting feature to note here is the dramatic increase in the temperature range of negative thermal expansion of ZnSe under hydrostatic compression. The negative thermal expansion can be understood as follows. At low T, the excited phonon modes are predominantly of TA type with negative $\gamma_{j,q}$ [see Eq. (54) and Fig. 8], giving negative values of α_a. Moreover, as shown above, the hydrostatic pressure leads to a decrease in the

frequency of the TA phonon modes and to an increase in that of the other modes. Thus, at high P and low T, the predominance of the TA phonon modes becomes increasingly more pronounced, leading to an increase in the range of T where α_a is negative and to a reduction in its calculated values. The calculated $C_V(T)$ of ZnSe is also in excellent agreement with experiment, and it is much less sensitive to pressure than α_a.
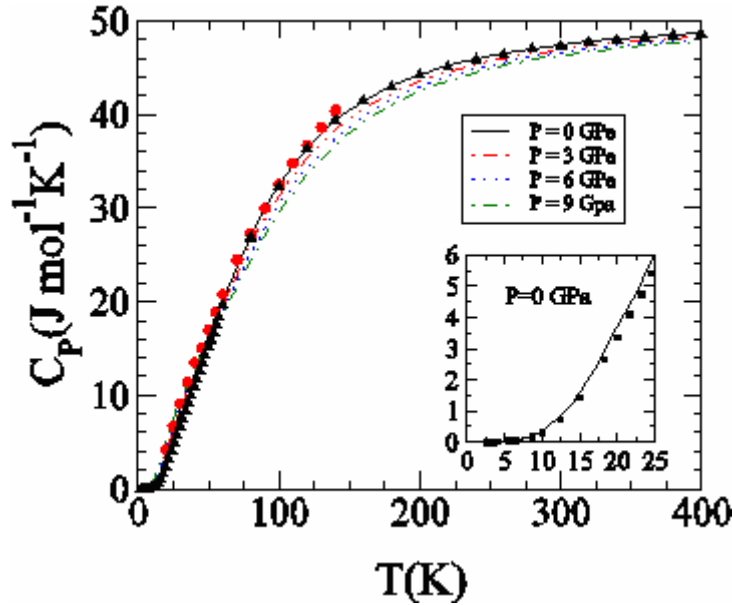
FIG. 10. As in Fig. 9, but for heat capacity at constant pressure. Triangles: NLCC calculations. Circles: experimental data of Ref. 96. Squares: experimental data of Ref. 97. Inset: data in the temperature range of 0–25 K, at zero P. (Taken from Ref. 40).

The presented phonon spectra and thermal properties of ZnSe can be considered as examples on the accuracy of the LDA calculations, described in Sec. III, for many physical and chemical properties of a wide range of systems.

VI. Wannier Functions: Recent Developments and Applications

As noted in Sec. I, the non-uniqueness property of the localized Wannier functions (WFs) has dramatically limited their applications. Thus, the most important development in this field is the introduction of unique maximally localized WFs (MLWFs), by Marzari and Vanderbilt [53]. The MLWFs have already found interesting applications [54-67]. In this section, we provide a brief description of MLWFs, and

focus on the novel bond ionicity scale based on the center of the MLWFs [67].

VI.A. Maximally localized Wannier functions

The electronic states in periodic systems are usually described in terms of extended Bloch orbitals

$$\varphi_{nk}(\boldsymbol{r}) = u_{nk}(\boldsymbol{r})e^{ik.r}, \qquad (55)$$

where $u_{n,\mathbf{k}}(\mathbf{r})$ are periodic functions with the periodicity of the crystal. The Bloch orbitals are characterized by two quantum numbers: the wave vector inside the first Brillouin zone (BZ), $\boldsymbol{k}$, and the band index n. An alternative representation is in terms of localized real-space orbitals or Wannier functions (WFs), $|\mathbf{R}n>$, which are characterized by real-space translation vectors $\mathbf{R}$ and n. The WFs can be

constructed from the extended Bloch orbitals according to

$$| \mathbf{R}n > = \frac{V_{cell}}{(2\pi)^3} \int_{BZ} | \varphi_{n,\mathbf{k}} > e^{i\zeta_n(\mathbf{k})-i\mathbf{k}.\mathbf{r}} d\mathbf{k}, \quad (56)$$

where $\zeta_n(\mathbf{k})$ is an arbitrary periodic phase factor in the reciprocal lattice. Such phase factors, which do not affect the physical properties extracted from Bloch's orbitals, lead to the non-uniqueness of the WFs.

Marzari and Vanderbilt [53] have exploited the above non-uniqueness property to construct MLWFs. This has been done by writing

$$| \mathbf{R}n > = \frac{V_{cell}}{(2\pi)^3} \int_{BZ} \sum_{m=1}^{N} U_{mn}^{(\mathbf{k})} | \varphi_{n,\mathbf{k}} > e^{-i\mathbf{k}.\mathbf{R}} d\mathbf{k}, (57)$$

where $U_{mn}^{(\mathbf{k})}$ are unitary matrices of dimension N (number of occupied states). Then, the optimal set of $U_{mn}^{(\mathbf{k})}$ is obtained by minimizing a spread function given as

$$\Omega = \sum_n < 0n | r^2 | 0n > - < 0n | \mathbf{r} | 0n >^2 . \quad (58)$$

The expectation value $\mathbf{r}_n = < 0n | \mathbf{r} | 0n >$ defines the centers of the MLWFs. An elegant iterative scheme for minimizing Ω has been introduced by Marzari and Vanderbilt [53].

In our work [67], we followed the procedure of Ref. 53 to construct the MLWFs of 32 $A^N B^{8-N}$ compounds, with $N = 1, 2, 3$ and 4, in their ground-state structures [diamond, zincblende (ZB), or rocksalt (RS)]. The considered systems consist of 3 of group-IV elemental solids in the diamond structure, the cubic phase of SiC, 15 III–V compounds in the ZB structure, 4 IIB–VI compounds in the ZB structure, 4 IIA–VI compounds in the RS structure and 4 I–VII compounds in the RS structure.

Let us first start with the elemental group-IV solids (Si, Ge and α-Sn) in the diamond structure. For such systems, there are four bonding MLWFs per primitive unit cell since there are eight valence electrons filling completely four valence bands. This means that there is a symmetric MLWF associated with each bond, as shown in Fig. 11, in the case of Si. The center of the MLWF coincides with that of the corresponding bond. The

relative position of the center of the MLWF is defined as $\beta = r_n / d$, where r_n is the distance between $\mathbf{r}_n$ and the position of the cation of the associated bond and d is the bond length. Thus, for elemental group-IV solids, $\beta = 0.5$.

For the $A^N B^{8-N}$ compounds crystallizing in the ZB structure, the mean features of the MLWFs are quite similar to those of the elemental group-IV solids. However, in the ZB form, the two atoms at the ends of each bond have different electronegativities, which leads to a partial charge transfer from the cation to the anion regions. This, in turn, shifts the center of the MLWFs away from the center of the bond toward the anion, as illustrated in Fig. 12, in the case of GaN. Therefore, the values of β of these systems are larger than 0.5. We have demonstrated (see next subsection) that there is a strong correlation between $(\beta - 0.5)$ and the bond ionicity [67], as expected. Based on this fact, an ionicity scale will be introduced in the next subsection.

For the more ionic I–VII and IIA–VI compounds crystallizing in the sixfold coordinate RS phase, the situation is quite different; the one-to-one correspondence between the bonding MLWFs and bonds breaks down. In the RS structure, the four bonding MLWFs, per primitive unit cell, correspond to six bonds. Because of the large bond ionicity of these compounds, one expects the MLWFs to be centered near the anions. Our calculations have shown that the centers of the MLWFs lie along four of the eight [111] directions of the cubic crystals, very close to the anions, as shown in Fig. 13, in the case of NaCl. It is interesting to note that, with respect to the anions, the MLWFs in the RS phase have the same orientation as those in the ZB phase (along the bonds of the latter structure). Moreover, it is meaningful to consider that each MLWF is a superposition of three somehow "optimized" σ-bond orbitals of the three neighboring bonds (see Fig. 13). Thus, each bond yields two thirds of an MLWF, which is the same ratio between the number of MLWFs and the bonds in the RS structure. To find the value of β of the relevant compounds, we consider one of the above "optimized" σ-bond orbitals and take its center to be the component of the center of any of the two associated MLWFs along the corresponding bond.
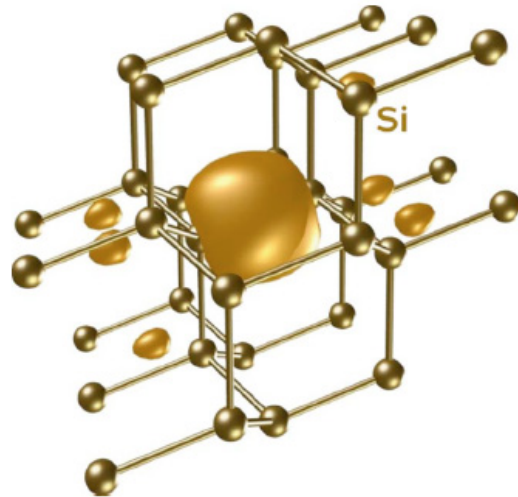
FIG. 11. An isosurface of a maximally localized Wannier function of Si in the diamond. (Taken from Ref. 67).
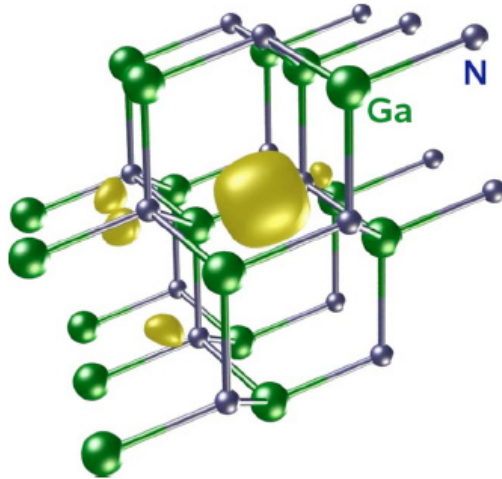
FIG. 12. An isosurface of a maximally localized Wannier function of GaN in the zinc-blende structure. (Taken from Ref. 67).
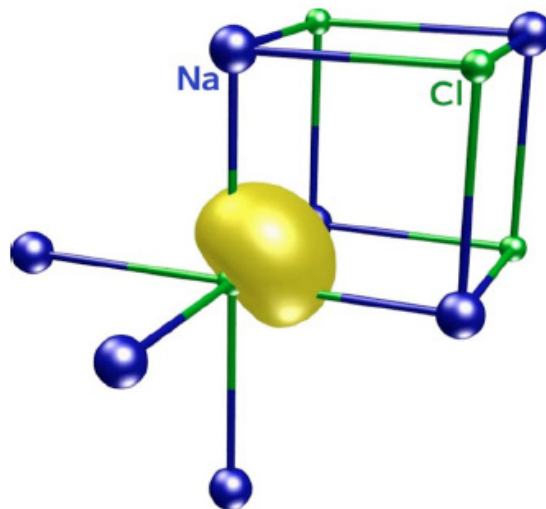
FIG. 13. An isosurface of a maximally localized Wannier function of NaCl in the rocksalt structure. (Taken from Ref. 67).

VI.B. A Novel Bond Ionicity Scale Based on the Centers of Mlwfs

As noted in the previous subsection, there is a strong correlation between the deviation of $\mathbf{r}_n$ from the bond center [expressed by $(\beta - 0.5)$] and the bond ionicity (see Fig. 14). This, in turn, shows that $(\beta - 0.5)$ can be used as a measure for the bond ionicity. To devise a bond ionicity scale based on $(\beta - 0.5)$, it is important to realize that we are dealing with a bond property in the solid phase of the material. Therefore, the concept of resonant bonds of Pauling [98] also applies to the present case. This implies that such an ionicity scale should also depend on the valency N and coordination number M. After several attempts, we found that the best ionicity scale takes the form

$$w_i = (2\beta - 1)^{(N/M)} . \qquad (59)$$

A remarkable feature of this ionicity scale is that it involves only physical constants.

The previous *ab initio* ionicity scales are extracted from either the charge density (Ref. 99), g, or band structure parameters (Ref. 100), f_i^*. It is worth noting that these are properties of the solid as a whole. The same can be said about the most famous empirical ionicity scale of Phillips [101], f_i, which is based on the dielectric theory of Phillips and Van Vechten. Thus, a major advantage of our ionicity scale is that it is directly derived from a bond related, see above.

A comparison between the present ionicity scale and previous empirical [101] and *ab initio* ones [99,100] is shown in Fig. 15. The important features to note from this figure are: (i) The quite large scattering of the previous values of bond ionicity. (ii) The w_i provides almost a best fit to the previously available values. This reflects the accuracy and reliability of the w_i bond ionicity scale. Moreover, we have shown [67] that the critical value of the bond ionicity that separates the fourfold (ZB or wurtzite) and sixfold (RS) coordinate structures is found to be of about 0.7.
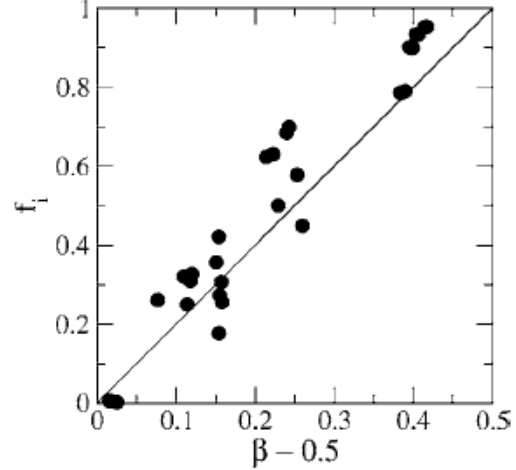
FIG. 14. The Phillips bond ionicity (f_i) vs ($\beta - 0.5$) for the considered $A^N B^{8-N}$ compounds. Those of the elemental group-IV solids are not shown. (Taken from Ref. 67).
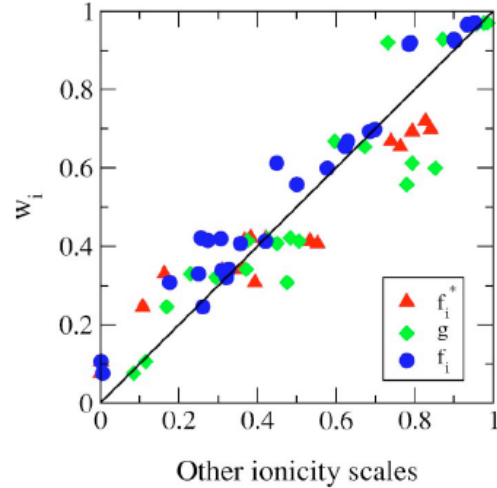
Fig. 15. The present bond ionicity w_i vs those of Phillips (Ref. 101), f_i, Garcia and Cohen (Ref. 99), g, and Christensen *et al.* (Ref. 100), f_i^*. (Taken from Ref. 67).

VII. Summary

Advances in modern computational electronic structure techniques, mainly based on Kohn-Sham density functional theory (KS-DFT), have made them the most attractive and widely used theoretical methods for investigating many properties of a wide range of systems. They are currently being used to tackle fundamental problems in physics, chemistry, geology, material science and biology. The great success of these theoretical approaches can be attributed to four main reasons.

(i) Their accuracy and high predictive power. This is demonstrated in this review article by presenting results in excellent agreement with experiment for the electronic structure, phonon spectra, dielectric and thermal properties of semiconductors. Moreover, these parameter free approaches enable us to get a deeper understanding and faithful explanation of the experimental results and allow us to study the properties of systems which are either unstable or not yet experimentally realized. This is particularly important when searching for new materials with specific properties and for investigating the behavior of the materials under extreme conditions which can't be obtained in the laboratory, such as the high temperature and pressure in the Earth's core.

(ii) The continuous progress in both basic theory and algorithms which increases the accuracy and efficiency of these methods and open the door for new applications.

(iii) The availability of a large variety of codes, which are rather easy to use and have many interesting and useful features.

(iv) The huge progress in the computer performance.

Providing a comprehensive account of these approaches and their developments and applications is far beyond the scope of any review article. Instead, this subject is introduced through a set of examples taken from my recent research work, which touch upon some important recent developments in this field, namely the exact-exchange formalism within KS-DFT, exact-exchange based quasi-particle GW calculations and maximally localized Wannier functions. This is in addition to the density functional perturbation theory. The basic theory behind these approaches is briefly described and some results are provided to demonstrate the accuracy and capabilities of these approaches. It should be noted that the presented results are obtained using programs to which we have added the new used features, namely the exact-exchange and maximally localized Wannier functions to the SPHINX code [102].

Acknowledgements

References

[1] Kohn, W. and Sham, L.J., Phys. Rev. A, 140 (1965) 1133.

[2] Hohenberg, P. and Kohn, W., Phys. Rev. B, 136 (1964) 864.

[3] Martin, R.M., Electronic Structure: Basic Theory and Practical Methods (Cambridge University Press, Cambridge, 2004).

[4] Perdew, J.P. and Zunger, A., Phys. Rev. B, 23 (1981) 5048.

[5] Godby, R.W., Schlüter, M. and Sham, L.J., Phys. Rev. B, 37 (1988) 10159.

[6] Kotliar, G. et al., Rev. Mod. Phys., 78 (2006) 865.

[7] Vogel, D., Krüger, P. and Pollmann, J., Phys. Rev. B, 54 (1996) 5495.

[8] Qteish, A., J. Phys.: Condens. Matter, 12 (2000) 5639.

[9] Langreth, D.C. and Mehl, M.J., Phys. Rev. B, 28 (1983) 1809.

[10] Städele, M., Majewski, J.A., Vogl, P. and Görling, A., Phys. Rev. Lett., 79 (1997) 2089.

[11] Städele, M., Moukara, M., Majewski, J.A., Vogl, P. and Görling, A., Phys. Rev. B, 59 (1999) 10031.

[12] Sahni, V., Gruenebaum, J. and Perdew, J.P., Phys. Rev. B, 26 (1982) 4371.

[13] Sharp, R.T. and Horton, G.K., Phys. Rev., 90 (1953) 317.

[14] Talman, J.D. and Shadwick, W.F., Phys. Rev. A, 14 (1976) 36.

[15] Qteish, A., Al-Sharif, A.I., Boeck, S., Neugebauer, J., Fuchs, M. and Scheffler, M., Phys. Rev. B, 72 (2005) 155317.

[16] Aulbur, W.G., Jönsson, L. and Wilkins, J.W., Solid State Phys., 54 (1999) 1.

[17] Rinke, P., Qteish, A., Nuegebauer, J., Froysoldt, C. and Scheffler, M., New Journal of Physics, 7 (2005) 126.

[18] Hedin, L., Phys. Rev., 139 (1965) A796.

[19] Hybertsen, M.S. and Louie, S.G., Phys. Rev. Lett., 55 (1985) 1418.

[20] Godby, R.W., Schlüter, M. and Sham, L.J., Phys. Rev. Lett., 56 (1986) 2415.

[21] Kotani, T. and van Schilfgaarde, M., Solid State Commun., 121 (2002) 476.

[22] Usuda, M., Hamada, N., Shiraishi, K. and Oshiyama, A., Jpn. J. Appl. Phys., 43 (2004) L407.

[23] Rohlfing, M., Krüger, P. and Pollmann, J., Phys. Rev. Lett., 75 (1995) 3489.

[24] Rohlfing, M., Krüger, P. and Pollmann, J., Phys. Rev. B, 57 (1998) 6485.

[25] Luo, W., Ismail-Beigi, S., Cohen, M.L. and Louie, S.G., Phys. Rev. B, 66 (2002) 195215.

[26] Qteish, A., Al-Sharif, A.I., Boeck, S., Neugebauer, J., Fuchs, M. and Scheffler, M., Computer Physics Comm., 169 (2005) 28.

[27] Rinke, P., Scheffler, M., Qteish, A., Winkelnkemper, M., Bimberg, D. and Nuegebauer, J., Appl. Phys. Lett., 89 (2006) 176919.

[28] Rinke, P., Winkelnkemper, M., Qteish, A., Bimberg, D., Nuegebauer, J., Scheffler, M., Phys. Rev. B, 77 (2008) 075202.

[29] Rinke, P., Qteish, A., Neugebauer, J., Freysoldt, C. and Scheffler, M., Phys. Stat. Sol. (b), 245 (2008) 929.

[30] Qteish, A., Rinke, P., Neugebauer, J. and Scheffler, M., Phys. Rev. B, 74 (2006) 245208.

[31] Qteish, A., Rinke, P., Neugebauer, J. and Scheffler, M., unpublished.

[32] Baroni, S., Giannozzi, P. and Testa, A., Phys. Rev. Lett., 59 (1987) 2662.

[33] Gonze, X., Allan, D.C. and Teter, M.P., Phys. Rev. Lett., 68 (1992) 3603.

[34] Gonze, X., Phys. Rev. B, 55 (1997) 10337.

[35] Gonze, X. and Lee, C., Phys. Rev. B, 55 (1997) 10355.

[36] Baroni, S., de Gironcoli, S., Dal Corso, A. and Giannozi, P., Rev. Mod. Phys., 73 (2001) 515.

[37] Hamann, D.R., Wu, X., Rabe, K.M. and Vanderbilt, D., Phys. Rev. B, 71 (2005) 035117.

[38] Wu, X., Vanderbilt, D., Hamann, D.R., Phys. Rev. B, 72 (2005) 035105.

[39] Aouissi, M., Hamdi, I., Meskini, N. and Qteish, A., Phys. Rev. B, 74 (2006) 054302.

[40] Hamdi, I., Aouissi, M., Qteish, A. and Meskini, N., Phys. Rev. B, 73 (2006) 174114.

[41] Tahri, S., Qteish, A., Al-Qasir, I. and Meskini, N., unpublished.

[42] Born, M. and Huang, K., Dynamical Theory of Crystal Lattices (Oxford University Press, New York, 1954).

[43] Carrier, P., Wentzcovitch, R. and Tsuchiya, J., Phys. Rev. B, 76 (2007) 064116.

[44] Wu, Z. and Wentzcovitch, R., Phys. Rev. B, 79 (2009) 104304.

[45] Grabowski, B., Ismer, L., Hickel, T. and Neugebauer, J., Phys. Rev. B, 79 (2009) 134106.

[46] Kunc, K. and Martin, R.M., in "*Ab initio* Calculations of Phonon Spectra", edited by J. T. Devreese, V. E. Van Doren and P. E. Van Camp (Plenum, New York, 1985), P. 65.

[47] Srivastava, G.P., Physics of Phonons (Taylor and Francis Group, New York, 1990).

[48] Fasolino, A., Molinari, E. and Kunc, K., Phys. Rev. B, 41 (1990) 8302.

[49] Qteish, A. and Molinari, E., Phys. Rev. B, 42 (1990) 7090.

[50] Ben Amar, A., Qteish, A. and Meskini, N., Phys. Rev. B, 53 (1996) 5372.

[51] Ben Amar, A., Qteish, A. and Meskini, N., Phys. Rev. B, 60 (1999) 6452.

[52] Wei, S. and Chou, M.Y., Phys. Rev. Lett., 69 (1992) 2799.

[53] Marzari, N. and Vanderbilt, D., Phys. Rev. B, 56 (1997) 12847.

[54] King-Smith, R.D. and Vanderbilt, D., Phys. Rev. B, 47 (1993) 1651.

[55] Vanderbilt, D. and King-Smith, R.D., Phys. Rev. B, 48 (1993) 4442.

[56] Resta, R., Rev. Mod. Phys., 66 (1994) 899.

[57] Williamson, A.J., Hood, R.Q. and Grossman, J.C., Phys. Rev. Lett., 87 (2001) 246406.

[58] Wu, X., Selloni, A. and Car, R., Phys. Rev. B, 79 (2009) 085102.

[59] Calzolari, A., Marzari, N., Souza, I. and Nardelli, M.B., Phys. Rev. B, 69 (2004) 035108.

[60] Usui, H., Arita, R. and Kurok, K., J. Phys.: Condens. Matter, 21 (2009) 064223.

[61] Ku, W., Rosner, H., Pickett, W.E. and Scalettar, R.T., Phys. Rev. Lett., 89 (2002) 167204.

[62] Schnell, I. and Kotliar, G., Phys. Rev. B, 65 (2002) 075103.

[63] Paul, I. and Kotliar, G., Phys. Rev. B, 67 (2003) 115131.

[64] Whittaker, D.M. and Croucher, M.P., Phys. Rev. B, 67 (2003) 085204.

[65] Silvestrelli, P.L., Phys. Rev. Lett., 180 (2008) 053002.

[66] Wahn, M. and Neugebauer, J., Phys. Stat. Sol. (b), 243 (2006) 1583.

[67] Abu-Farsakh, H. and Qteish, A., Phys. Rev. B, 75 (2007) 085201.

[68] Payne, M.C., Teter, M.P., Allan, D.C., Arias, T.A. and Joannopoulos, J.D., Rev. Mod. Phys., 64 (1992) 1045.

[69] Fock, V., Z. Phys., 63 (1930) 855.

[70] Jones, R.O. and Gunnarsson, O., Rev. Mod. Phys., 76 (1989) 681.

[71] Staroverov, V.N., Scuseria, G.E., Tao, J. and Perdew, J.P., Phys. Rev. B, 69 (2004) 075102.

[72] Däne, M. et al., J. Phys.: Condens. Matter, 21 (2009) 045604, and references therein.

[73] Filippetti, A. and Spaldin, N.A., Phys. Rev. B, 67 (2003) 125109.

[74] Droghetti, A., Pemmaraju, C.D. and Sanvito, S., Phys. Rev. B, 78 (2008) 140404(R).

[75] Anisimov, V.I., Aryasetiawan, F. and Lichtenstein, A.I., J. Phys.: Condens. Matter, 9 (1997) 767.

[76] Becke, A.D., J. Chem. Phys., 98 (1993) 1372.

[77] Casida, M.E., Phys. Rev. A, 51 (1995) 2005.

[78] Kümmel, S. and Perdew, J.P., Phys. Rev. B, 68 (2003) 035103.

[79] Gross, E., Runge, E. and Heinonen, O., Many-Particle Theory (Hilger, Bristol, 1991).

[80] Landau, L.D., Sov. Phys.—JETP, 3 (1957) 920; Sov. Phys.—JETP, 5 (1957) 101; Sov. Phys.— JETP, 35 (1959) 70.

[81] Magyar, R.J., Fleszar, A. and Gross, E.K.U., Phys. Rev. B, 69 (2004) 045111.

[82] Wu, J. et al., Appl. Phys. Lett., 80 (2002) 3967.

[83] Davydov, V.Y. et al., Phys. Status Solidi B, 229 (2002) R1.

[84] Nanishi, Y., Saito, Y. and Yamaguchi, T., Jpn. J. Appl. Phys., 42 (2003) 2549.

[85] Wu, J. et al., Phys. Rev. B, 66 (2002) 201403.

[86] Walukiewicz, W. et al., J. Cryst. Growth, 269 (2004) 119.

[87]The ABINIT code is a common project of the Université Catholique de Louvin, Corning Incorporated, and other contributors, URL http://www.abinit.org.

[88]The knowledge of $\{\varphi^{(n)}\}$ allows the calculation of the total energy derivatives up to the (2n+1) order.

[89]Sternheimer, R.M., Phys. Rev., 96 (1954) 951.

[90]Hennion, H., Moussa, F., Pepy, G. and Kunc, K., Phys. Lett. A, 35 (1971) 376.

[91]Louie, S.G., Froyen, S. and Cohen, M.L., Phys. Rev. B, 26 (1982) 1738.

[92]Callen, H.B., Thermodynamics and an Introduction to Thermostatistics (Wiley, New York, 1985).

[93]Karch, K., Pavone, P., Windl, W., Schütt, O. and Strauch, D., Phys. Rev. B, 50 (1994) 17054.

[94]Smith, T.F. and White, G.K., J. Phys. C, 8 (1975) 2031.

[95]Novikova, S.I., Fiz. Tverd. Tela (Leningrad) 2 (1960) 2341. [Sov. Phys. Solid State, 2 (1976) 2087]; 3 (1976) 178 [3 (1976) 129]; 5 (1963) 2138 [5 (1964) 1558]; 1 (1959) 1841 [1 (1960) 1687].

[96]Irwin, J.C. and LaCombe, J., J. Appl. Phys., 45 (1974) 567.

[97]Birch, J.A., J. Phys. C, 8 (1975) 2043.

[98]Phillips, J.C., Bonds and Bands in Semiconductors (Academic Press, New York, 1973).

[99]Garcia, A. and Cohen, M.L., Phys. Rev. B, 47 (1993) 4215.

[100]Christensen, N.E., Satpathy, S. and Pawlowska, Z., Phys. Rev. B, 36 (1987) 1032.

[101]Phillips, J.C., Rev. Mod. Phys., 42 (1970) 317.

[102]www.sphinxlib.de.